High-Resolution DOA Estimation of True Target by Rejecting Ghost Targets Effect
Initial Results of IAA-GTR

Ryuhei Takahashi
Information Technology R&D Center,
Mitsubishi Electric Corporation, Kamakura, Japan
Email: Takahashi.Ryuhei@ab.MitsubishiElectric.co.jp

Pu (Perry) Wang
Mitsubishi Electric Research Laboratories (MERL),
Cambridge, MA, USA
Email: pwang@merl.com

***Abstract*—This paper presents a high-resolution angle estimation method, IAA-GTR (Iterative Adaptive Approach - Ghost Target Rejection), to address ghost targets caused by multipath propagation. The method is particularly relevant for radar applications in autonomous driving and indoor monitoring. It operates on a MIMO (Multiple Input, Multiple Output) radar by first applying IAA on the receive-array data, generating a projection matrix to remove multipath signals. This results in the estimation of the DOA (Direction-of-Arrival) of only the true target using IAA on the MIMO-array data. Computer simulations with a typical MIMO radar setup demonstrated the effectiveness of the proposed method in accurately estimating the true target's DOA without being affected by ghost targets.**

***Index Terms*—radar, ghost targets, multipath.**

I. Introduction

The application of millimeter-wave radar is growing in fields such as autonomous driving[1][2][3], indoor monitoring[4][5], related sectors. However, when used in highway, urban, or indoor environments, multipath propagation through surrounding objects such as walls, barriers, and guardrails can occur, leading to the emergence of "ghost targets" which mimic the behavior of actual targets in the angle-range-Doppler data, despite the absence of a physical target, i.e. "true target". This can lead to a degradation in the accuracy and reliability of the millimeter-wave radar[1][2][3].

The elimination of ghost targets poses a substantial challenge in the development of advanced millimeter-wave radar, as it is critical to avoid malfunctions in higher-level systems. Various methods have been studied to solve the ghost target problem[6][7][8][9][10]. A method for monostatic radar that does not require prior environmental information or a training dataset is a clear advantage due to its versatility. Furthermore, the removal of ghost targets within a single frame is crucial in responding to dynamic changes in the propagation environment and reducing the computational burden associated with downstream tasks[11][12][13][14].

In this regard, there is a method for utilizing the angle difference between the direct-path and the multipath signal in the single frame data by measuring the DOD (Direction-of-Departure) and DOA from the received signal of the MIMO radar, commonly used in millimeter-wave radar. Conventional beamformers for simultaneous DOD and DOA measurement suffer from low angle resolution and high sidelobes[15][16]. High-resolution methods such as IAA (Iterative Adaptive Approach) [17] have been introduced to produce high-resolution DOD-DOA spectral maps with low sidelobes [18][19], but none of the methods address the angle ambiguity problem[16][20] when using a MIMO radar with a sparse transmit-array generating grating lobes. To address this, [21] proposes using the product of the DOD-DOA spectrum map and its transposed map obtained via MVDR (Minimum Variance Distortionless Response) to mitigate angular ambiguity, though its effectiveness under conditions with grating lobes on the diagonal axis on the map is unknown.

Recently, the ESTAR (Estimation of Two-way Angle by MIMO Radar) method has been proposed to solve the angle ambiguity problem[20][22]. ESTAR has proven effective in clearly separating the direct-path and multipath signals based on the difference in the two-way angles, i.e., the combination of the DOD and DOA. However, as a beamformer-based method, ESTAR also generates high sidelobes and a wide mainlobe. Given these considerations, it is evident that a high-resolution angle estimation, such as IAA, can be employed to remove the sidelobes and obtain the two-way angle.

However, there is a challenge concerning the computational cost of executing IAA with ESTAR due to the two-dimensional angle grid search, as we will elaborate in II-C. In this paper, we propose a method for obtaining the one-dimensional high-resolution DOA spectrum of only the true target while eliminating the effects of ghost targets. To reduce the computational cost, the proposed method involves acquiring the DOA of multipath signals from the receive-array data prior to applying MIMO waveform matched filters. Subsequently, the projection matrix obtained from this process is utilized to remove the multipath signals from the MIMO-array data after the waveform matched filters. This results in the direct-path signal being the sole remaining component in the received vector. Employing one-dimensional IAA subsequently allows for the extraction of the high-resolution DOA spectrum of the true target while effectively eliminating the ghost targets.

II. Selective DOA Estimation

A. Signal Model

In the standard radar signal processing pipeline for millimeter-wave MIMO radar, signal detection is performed for the range-Doppler response in each MIMO array channel. Then, beamforming is performed for the detected range-Doppler cells to estimate the DOA. By defining the arbitrary DOD and DOA as u_1 and u_2, respectively, the corresponding MIMO-array response vector is expressed as $\mathbf{a}(u_1, u_2) \in \mathbb{C}^{M\times 1}$, where M is the number of MIMO-array channels. The relationship between the transmit-array response vector $\mathbf{a}_{\mathrm{T}}(u_1) \in \mathbb{C}^{M_{\mathrm{T}}\times 1}$ and the receive-array response vector $\mathbf{a}_{\mathrm{R}}(u_2) \in \mathbb{C}^{M_{\mathrm{R}}\times 1}$, where M_{T} and M_{R} are the number of transmit-array channels and receive-array channels, respectively, is $\mathbf{a}(u_1, u_2) = \mathbf{a}_{\mathrm{T}}(u_1) \otimes \mathbf{a}_{\mathrm{R}}(u_2)$, where $\otimes$ represents the Kronecker product.

Consider the received MIMO-array data $\mathbf{y} \in \mathbb{C}^{M\times 1}$ in a detected range-Doppler cell in the geometry shown in Fig. 1. The received data $\mathbf{y}$ is given as

$$\mathbf{y} = \mathbf{a}(u_{\mathrm{D}}, u_{\mathrm{D}})\, s_{\mathrm{D}} + \mathbf{b}(u_{\mathrm{A}}, u_{\mathrm{B}})\, s_{\mathrm{M}}, \tag{1}$$

where s_{D} and s_{M} are the complex amplitudes of the direct-path and multipath signal, respectively, and u_{D} is the DOD and DOA of the direct-path signal indicated by green color arrows. The multipath signal has a propagation path with u_{A} of DOD and u_{B} of DOA indicated by blue color arrows, and the reverse propagation path by red color arrows. The pair of u_{A} and u_{B} is therefore defined as the two-way angle [20], and the following two-way multipath array response vector is introduced as $\mathbf{b}(u_{\mathrm{A}}, u_{\mathrm{B}}) = \mathbf{a}(u_{\mathrm{A}}, u_{\mathrm{B}}) + \mathbf{a}(u_{\mathrm{B}}, u_{\mathrm{A}})$.

Next, for any two arbitrary angles u and v, the direct-path array response vector $\mathbf{a}(u, u)$ corresponding to the number of N angle grids that satisfy $u = v$ is stored as a column vector in the dictionary matrix, which is the direct-path array manifold $\mathbf{A}_{\mathrm{D}}$. The dictionary matrix that stores the two-way multipath array response vector $\mathbf{b}(u, v)$ corresponding to $\frac{N(N-1)}{2}$ angle grids for both angles that satisfy $u \neq v$ as a column vector is the two-way multipath propagation array manifold $\mathbf{B}_{\mathrm{M}}$. By utilizing the two dictionary matrices, (1) can be rewritten as

$$\mathbf{y} = \begin{bmatrix}\mathbf{A}_{\mathrm{D}} & \mathbf{B}_{\mathrm{M}}\end{bmatrix}\begin{bmatrix}\mathbf{x}_{\mathrm{D}} \\ \mathbf{x}_{\mathrm{M}}\end{bmatrix} \tag{2}$$

$$= \mathbf{A}_{\mathrm{D}}\mathbf{x}_{\mathrm{D}} + \mathbf{B}_{\mathrm{M}}\mathbf{x}_{\mathrm{M}}, \tag{3}$$

where $\mathbf{x}_{\mathrm{D}} \in \mathbb{C}^{N\times 1}$ and $\mathbf{x}_{\mathrm{M}} \in \mathbb{C}^{\frac{N(N-1)}{2}\times 1}$ are the direct-path and the multipath signal vector respectively. It is evident that s_{D} and s_{M} are contained in $\mathbf{x}_{\mathrm{D}}$ and $\mathbf{x}_{\mathrm{M}}$ respectively.

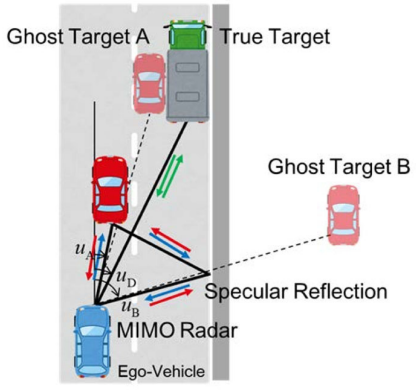

Fig. 1. Observation geometry of MIMO radar. Multipath propagation by blue and red arrows and direct-path propagation by green arrows are received in a single range Dopper cell.

B. Conventional Methods

Conventional DOA estimation extracts the peak of the beamforming output $\mathbf{x}_{\mathrm{BF}}$ as shown in (4), where the column vector of $\mathbf{A}_{\mathrm{D}}$ is used as the beam weight on $\mathbf{y}$.

$$\mathbf{x}_{\mathrm{BF}} = {\mathbf{A}_{\mathrm{D}}}^{\mathrm{H}}\mathbf{A}_{\mathrm{D}}\mathbf{x}_{\mathrm{D}} + {\mathbf{A}_{\mathrm{D}}}^{\mathrm{H}}\mathbf{B}_{\mathrm{M}}\mathbf{x}_{\mathrm{M}}. \tag{4}$$

As (4) clearly shows, $\mathbf{x}_{\mathrm{BF}}$ includes the direct-path signal response, $\mathbf{A}_{\mathrm{D}}^{\mathrm{H}}\mathbf{A}_{\mathrm{D}}\mathbf{x}_{\mathrm{D}}$, as well as the sidelobe response, ${\mathbf{A}_{\mathrm{D}}}^{\mathrm{H}}\mathbf{B}_{\mathrm{M}}\mathbf{x}_{\mathrm{M}}$, of the multipath signals. This sidelobe response corresponds to the ghost target that appears in the conventional DOA spectrum. Due to this characteristic, the angle that gives the peak of the ghost target generally does not match the DOAs of the multipath signals. ESTAR[20] uses the matrix $\begin{bmatrix}\mathbf{A}_{\mathrm{D}} & \mathbf{B}_{\mathrm{M}}\end{bmatrix}$ as the beam weight to calculate the beamforming output of (3). This allows for the separation of the direct-path signal response $\mathbf{A}_{\mathrm{D}}^{\mathrm{H}}\mathbf{A}_{\mathrm{D}}\mathbf{x}_{\mathrm{D}}$ and the multipath signal response $\mathbf{B}_{\mathrm{M}}^{\mathrm{H}}\mathbf{B}_{\mathrm{M}}\mathbf{x}_{\mathrm{M}}$ on the ESTAR spectrum map.

IAA[17] is an iterative algorithm based on weighted least squares. It uses the reconstructed signal vector to form the correlation matrix. Then, it calculates the inverse matrix to iteratively update the signal vector. Therefore the computational cost of IAA is $O\left(M^3 + M^2 N_{\mathrm{g}}\right)$ per iteration, where N_{g} denotes the number of dimensions of the signal vector, or the number of angle grids. In many cases of millimeter-wave radar, M is significantly smaller than N_{g}, i.e. $M \ll N_{\mathrm{g}}$. This makes the impact of N_{g}, which comes from the correlation matrix operation, difficult to disregard.

C. Proposed IAA-GTR

When applying IAA to the signal model in (2), the signal vector to be reconstructed is $\begin{bmatrix}{\mathbf{x}_{\mathrm{D}}}^{\mathrm{T}} & {\mathbf{x}_{\mathrm{M}}}^{\mathrm{T}}\end{bmatrix}^{\mathrm{T}}$, and $N_{\mathrm{g}} = N + \frac{N(N-1)}{2}$. The fundamental challenge of the ghost target problem is to estimate the DOA of the direct-path signal while rejecting the interference by the multipath signal, rather than estimating the two-way angles of the multipath signal. Recognizing that the direct-path signal s_{D} is contained in the signal vector $\mathbf{x}_{\mathrm{D}}$, it is sufficient to limit the signal vector to be reconstructed by IAA to $\mathbf{x}_{\mathrm{D}}$ alone. This approach significantly reduces the computational cost of IAA from $O\left(M^3 + M^2\left(\frac{N^2+N}{2}\right)\right)$ to $O\left(M^3 + M^2 N\right)$.

The proposed IAA-GTR is a method for obtaining the DOA spectrum of only the true target while eliminating the effects of ghost targets. To this end, the proposed method involves acquiring the DOAs of multipath signals from the

receive-array data before MIMO waveform matched filters. Subsequently, the projection matrix $\mathbf{P}$ obtained from this process is utilized to remove the multipath signals from the MIMO-array data $\mathbf{y}$. This results in the direct-path signal being the sole remaining component in $\mathbf{Py}$. Employing one-dimensional IAA subsequently allows for the extraction of the high-resolution DOA spectrum of the true target, i.e., direct-path signal, while effectively eliminating the ghost targets.

In order to remove the multipath propagation signals contained in (1), the receive-array data $\mathbf{y}_{\mathrm{R}} \in \mathbb{C}^{M_{\mathrm{R}} \times 1}$ before the MIMO waveform matched filters is modeled as,

$$\mathbf{y}_{\mathrm{R}} = \mathbf{a}_{\mathrm{R}}(u_{\mathrm{D}})\, s_{\mathrm{D}}^{(\mathrm{R})} + (\mathbf{a}_{\mathrm{R}}(u_{\mathrm{A}}) + \mathbf{a}_{\mathrm{R}}(u_{\mathrm{B}}))\, s_{\mathrm{M}}^{(\mathrm{R})} \tag{5}$$

$$= \mathbf{A}_{\mathrm{R}}\mathbf{x}_{\mathrm{R}} \tag{6}$$

where $s_{\mathrm{D}}^{(\mathrm{R})}$ and $s_{\mathrm{M}}^{(\mathrm{R})}$ are the complex amplitudes of the direct-path and multipath signal in the receive-array respectively. $\mathbf{A}_{\mathrm{R}}$ is the receive-array manifold matrix defined similarly to $\mathbf{A}_{\mathrm{D}}$. $\mathbf{x}_{\mathrm{R}} \in \mathbb{C}^{N \times 1}$ is the signal vector containing $s_{\mathrm{D}}^{(\mathrm{R})}$ and $s_{\mathrm{M}}^{(\mathrm{R})}$.

Applying IAA to $\mathbf{y}_{\mathrm{R}}$ results in the estimation of u_{D}, u_{A}, and u_{B}[1]. However, the identification of the three DOAs as direct-path signals or multipath signals remains unknown. The characteristics of multipath propagation, where the two signals propagate in opposite directions along the same path, indicate that one of the three DOAs may be a direct-path signal, while the other two could be multipath signals. This scenario can be classified into three combinations of the two-way angle, depending on the angles involved: $(u_{\mathrm{A}}, u_{\mathrm{B}})$, $(u_{\mathrm{A}}, u_{\mathrm{D}})$, and $(u_{\mathrm{D}}, u_{\mathrm{B}})$. Additionally, there are cases where all three DOAs are direct-path signals. The proposed method assumes that two-way multipath propagation is occurring. As there are three combinations as described above, the ESTAR spectrum value is calculated for each of these using (11) in [20]. A combination that gives the largest values is then selected as the two-way angle for the multipath propagation. If $(u_{\mathrm{A}}, u_{\mathrm{B}})$ is selected, the following projection matrix $\mathbf{P}$ is calculated.

$$\mathbf{P} = \mathbf{I} - \mathbf{b}(u_{\mathrm{A}}, u_{\mathrm{B}}) \left(\mathbf{b}^{\mathrm{H}}(u_{\mathrm{A}}, u_{\mathrm{B}})\, \mathbf{b}(u_{\mathrm{A}}, u_{\mathrm{B}})\right)^{-1} \mathbf{b}^{\mathrm{H}}(u_{\mathrm{A}}, u_{\mathrm{B}}) \tag{7}$$

The next step is to multiply the projection matrix $\mathbf{P}$ with the MIMO-array vector $\mathbf{y}$. This results in the received signal vector $\mathbf{y}_{\mathrm{P}}$, from which the multipath signal has been removed.

$$\mathbf{y}_{\mathrm{P}} = \mathbf{P}\mathbf{A}_{\mathrm{D}}\mathbf{x}_{\mathrm{D}} \tag{8}$$

The only unknown signal vector contained in $\mathbf{y}_{\mathrm{P}}$ is $\mathbf{x}_{\mathrm{D}}$. Finally, performing a one-dimensional search of N angle grids using IAA will yield a high-resolution DOA spectrum of only the direct-path signal, i.e., the true target, excluding the effects of ghost targets. The algorithm for the proposed IAA-GTR is summarized in Algorithm 1 [2].

[1]It should be noted that this estimation is subject to an estimation error; however, it will be ignored in the interest of simplifying the discussion.

[2]The scenarios under current discussion involve three DOAs obtained from the receive-array signal vector $\mathbf{y}_{\mathrm{R}}$. Even if the number of DOAs exceeds three, the projection matrix can be obtained similarly, but the process will be more complicated. We plan to report the details in the future.

Algorithm 1 Proposed IAA-GTR

Input: $\mathbf{y}$ and $\mathbf{y}_{\mathrm{R}}$

Output: $\mathbf{x}_{\mathrm{D}}$

1: Apply IAA to $\mathbf{y}_{\mathrm{R}}$ to reconstruct $\mathbf{x}_{\mathrm{R}}$ and extract up tp three peaks from $\mathbf{x}_{\mathrm{R}}$.
2: **if** $N_{\mathrm{p}} \geq 2$ where N_{p} is the number of peaks **then**
3: Find all combinations of angles, and set the combination that gives the highest ESTAR value as the two-way angle.
4: Calculate $\mathbf{P}$ by (7) to obtain $\mathbf{y}_{\mathrm{P}}$ by (8).
5: Apply IAA to $\mathbf{y}_{\mathrm{P}}$ to reconstruct signal vector $\mathbf{x}_{\mathrm{D}}$.
6: **else**
7: No multipath propagation is occurring. Apply IAA to $\mathbf{y}_{\mathrm{P}}$ by (8), where $\mathbf{P} = \mathbf{I}$ to reconstruct signal vector $\mathbf{x}_{\mathrm{D}}$.
8: **end if**

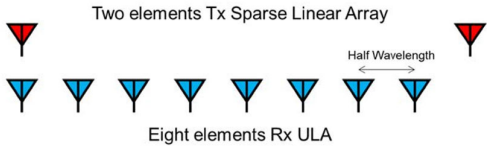

Fig. 2. Array configuration of the 77 GHz MIMO radar with a sparse linear Tx array and a uniform linear Rx array.

III. Computar Simulation

A. Setup

As shown in Fig. 2, the 77 GHz MIMO radar is considered where the receive-array is an eight-element uniform linear array with half-wavelength spacing, and the transmit-array is a sparse array with two elements at each end of the receive-array. The receiver noise is set to an average power of 0 dB, and the signal power is set to 20 dB for both the direct and multipath signals. Scenario 1 is a multipath propagation situation with two-way angle at (-45 deg, 20 deg). Fig. 3 shows the ESTAR map for Scenario 1, and it is clear that the maximum peak indicated by the white square appears at the set angles. An important observation is the sidelobe distribution, which extends to the diagonal axis of the ESTAR map where the actual DOA spectrum is observed. As described in II-A, this sidelobe response in the vicinity of -45 deg and 20 deg on the diagonal axis becomes a ghost target. In Scenario 2, a direct-path signal arriving from 0 deg is added to Scenario 1. The corresponding ESTAR map is shown in Fig. 4. Compared to Fig. 3, the sidelobe distribution is more complicated. It is easy to imagine that it would be difficult to distinguish between the mainlobe and sidelobes in the case of unknown propagation conditions, especially when there is a large difference in power between the signals.

B. Results

Fig. 5 shows the IAA spectrum of the receive-array in Scenario 1. There are two DOAs due to multipath propagation, and the two peaks in the IAA spectrum correspond to the -45 deg and 20 deg of expected DOAs. Then, the projection matrix $\mathbf{P}$ in (7) was obtained using the estimated DOAs. As illustrated in Fig. 6, the IAA spectrum of the received signal

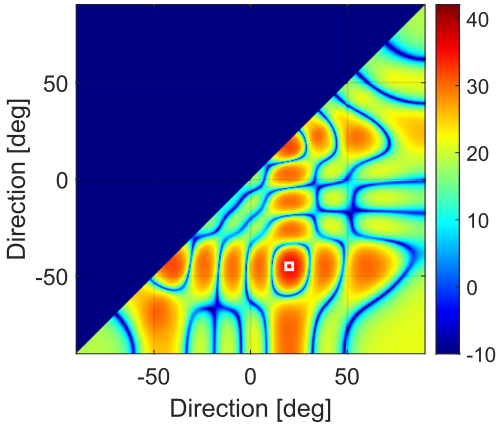

Fig. 3. ESATR spectrum map when only multipath signals are received. The two-way angle of the multipath signals is indicated by a white square.

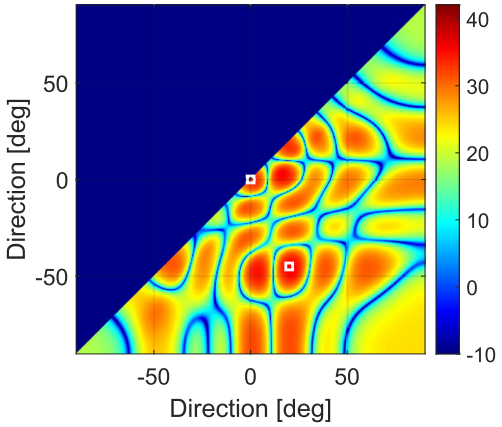

Fig. 4. ESATR spectrum map when direct-path and multipath signals are received. Respective two-way angles are indicated by a white square.

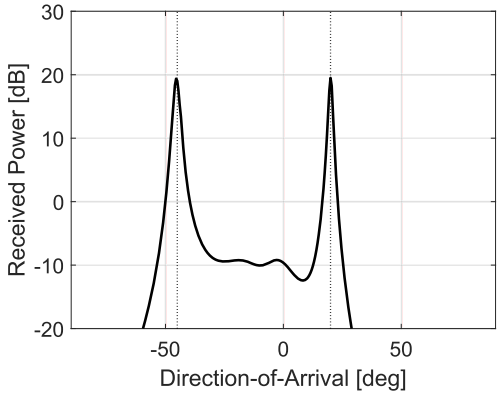

Fig. 5. DOA spectrum of the receive-array using IAA when only multipath signals are received. Two peaks correspond to the DOA of the multipath signal by the dotted line. The average noise power is at 0 dB.

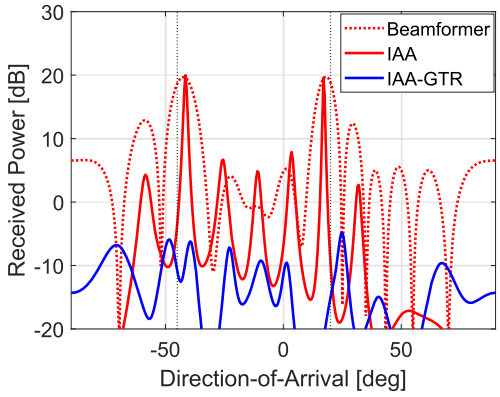

Fig. 6. DOA spectrum of the MIMO-array when only multipath signals are received. The IAA-GTR spectrum in the blue does not produce any ghost targets. In contrast, the conventional beamformer and IAA spectrum in the red dotted and solid lines, respectively, produce the ghost targets in the vicinity of the DOA of the multipath signal by the black dotted line. The average noise power is at 0 dB.

vector $\mathbf{y}_P$, which was obtained by multipath signal removal using the projection matrix $\mathbf{P}$ in (7), is shown in blue. The proposed IAA-GTR spectrum does not produce any ghost targets in the vicinity of the DOA of the multipath signal, as shown by the black dotted line. In contrast, the spectrum obtained using the conventional beamformer and IAA (shown as a red dotted line and red solid line, respectively) produces strong responses in the vicinity of the DOA of the multipath signal and therefore observes ghost targets.

Fig. 7 shows the IAA spectrum of the receive-array in Scenario 2. There is direct-path propagation in addition to multipath propagation, and the three peaks in the IAA spectrum correspond to those DOAs. There are three combinations of the two-way angles of multipath signals. Based on the ESTAR spectrum value, the two-way angle was estimated to be (20 deg, -45 deg). The projection matrix $\mathbf{P}$ was obtained using (7), and multipath signal removal was then performed using (8). The blue solid line in Fig. 8 is the DOA spectrum of the proposed IAA-GTR obtained in this way. The spectrum shows a peak that matches the DOA of the direct-path signal, indicated by the solid black line, but does not show a peak in the vicinity of the DOA of the multipath signal, indicated by the dotted black line, where the ghost target appears. In contrast, the DOA spectra of the conventional beamformer and IAA, indicated by the red dotted and solid lines, respectively, show a peak that matches the DOA of the direct-path signal as well as strong responses in the vicinity of the DOAs of the multipath signals, generating the ghost target.

IV. Concluding Remarks

In this paper, we proposed the IAA-GTR, which estimates the angle of the true target while rejecting ghost targets by searching for the one-dimensional DOA spectrum. We reported initial results on the basic operation of IAA-GTR. As described in the paper, further evaluation of the proposed method will be carried out in scenarios involving more complicated propagation. In addition, the robustness of the proposed

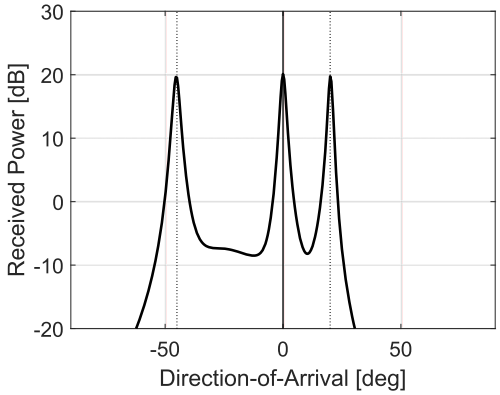

Fig. 7. DOA spectrum of the receive-array using IAA when direct-path and multipath signals are received. Two peaks correspond to the DOA of the multipath signal by the dotted line, and one peak corresponds to the DOA of the direct-path signal shown by the solid line. However, the identification of the three DOAs as direct-path or multipath is unclear from the spectrum. The average noise power is at 0 dB.

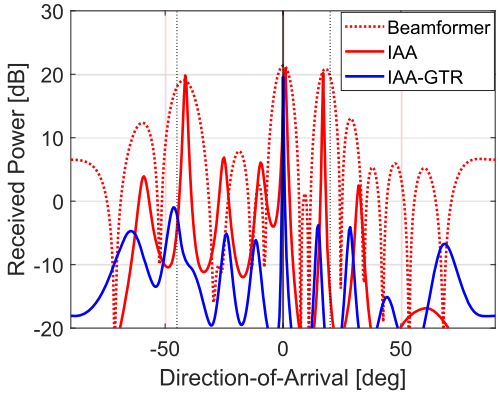

Fig. 8. DOA spectrum of the MIMO-array when direct-path and multipath signals are received. The IAA-GTR spectrum in the blue shows a peak that matches the DOA of the true target by the solid black line, but does not produce any ghost targets. In contrast, the conventional beamformer and IAA spectrum in the red dotted and solid lines, respectively, produce the ghost targets in the vicinity of the DOA of the multipath signal by the black dotted line. The average noise power is at 0 dB.

method will be evaluated by considering the impact of the error in the DOA in the IAA of the receive array on the calculation of the projection matrix. Most importantly, the proposed method will be evaluated using experimental data.

References

[1] I. Bilik, O. Longman, S. Villeval, and J. Tabrikian, "The rise of radar for autonomous vehicles: Signal processing solutions and future research directions," *IEEE Signal Processing Magazine*, vol. 36, no. 5, pp. 20–31, 2019.

[2] S. Sun, A. P. Petropulu, and H. V. Poor, "MIMO radar for advanced driver-assistance systems and autonomous driving: Advantages and challenges," *IEEE Signal Processing Magazine*, vol. 37, no. 4, pp. 98–117, 2020.

[3] F. Engels, P. Heidenreich, M. Wintermantel, L. Stäcker, M. Al Kadi, and A. M. Zoubir, "Automotive radar signal processing: Research directions and practical challenges," *IEEE Journal of Selected Topics in Signal Processing*, vol. 15, no. 4, pp. 865–878, 2021.

[4] M. Rahman, R. Yataka, S. Kato, P. Wang, P. Li, A. Cardace, and P. Boufounos, "MMVR: Millimeter-wave multi-view radar dataset and benchmark for indoor perception," in *The 18th European Conference on Computer Vision (ECCV) 2024*, 2024.

[5] A. Gharamohammadi, A. Khajepour, and G. Shaker, "In-vehicle monitoring by radar: A review," *IEEE Sensors Journal*, vol. 23, no. 21, pp. 25 650–25 672, 2023.

[6] C. Liu, S. Liu, C. Zhang, Y. Huang, and H. Wang, "Multipath propagation analysis and ghost target removal for FMCW automotive radars," in *IET International Radar Conference (IET IRC 2020)*, vol. 2020, 2020, pp. 330–334.

[7] O. Longman, S. Villeval, and I. Bilik, "Multipath ghost targets mitigation in automotive environments," in *2021 IEEE Radar Conference (RadarConf21)*, 2021, pp. 1–5.

[8] L. Li and J. L. Krolik, "Simultaneous target and multipath positioning with MIMO radar," in *IET International Conference on Radar Systems (Radar 2012)*, 2012, pp. 1–6.

[9] R. Feng, E. De Greef, M. Rykunov, S. Pollin, A. Bourdoux, and H. Sahli, "Multipath ghost recognition and joint target tracking with wall estimation for indoor MIMO radar," *IEEE Transactions on Radar Systems*, vol. 2, pp. 154–164, 2024.

[10] Y. Jin, R. Prophet, A. Deligiannis, I. Weber, J.-C. Fuentes-Michel, and M. Vossiek, "Comparison of different approaches for identification of radar ghost detections in automotive scenarios," in *2021 IEEE Radar Conference (RadarConf21)*, 2021, pp. 1–6.

[11] R. Yataka, P. P. Wang, P. Boufounos, and R. Takahashi, "Multi-view radar detection transformer with differentiable positional encoding," in *ICASSP 2025 - 2025 IEEE International Conference on Acoustics, Speech and Signal Processing (ICASSP)*, 2025, pp. 1–5.

[12] R. Yataka, P. Wang, P. Boufounos, and R. Takahashi, "Sira: Scalable inter-frame relation and association for radar perception," in *2024 IEEE/CVF Conference on Computer Vision and Pattern Recognition (CVPR)*, 2024, pp. 15 024–15 034.

[13] R. Yataka, A. Cardace, P. Wang, P. Boufounos, and R. Takahashi, "RETR: Multi-view radar detection transformer for indoor perception," in *NeurIPS*, 2024.

[14] R. Yataka, P. Wang, P. Boufounos, and R. Takahashi, "Multi-view radar detection transformer with differentiable positional encoding," in *ICASSP*, Apr. 2025.

[15] F. Engels, M. Wintermantel, and P. Heidenreich, "Automotive MIMO radar angle estimation in the presence of multipath," in *2017 European Radar Conference (EURAD)*, 2017, pp. 82–85.

[16] O. Biallawons and J. H. G. Ender, "Multipath detection by using space-space adaptive processing (SSAP) with MIMO radar," in *2018 International Conference on Radar (RADAR)*, 2018, pp. 1–4.

[17] T. Yardibi, J. Li, P. Stoica, M. Xue, and A. B. Baggeroer, "Source localization and sensing: A nonparametric iterative adaptive approach based on weighted least squares," *IEEE Transactions on Aerospace and Electronic Systems*, vol. 46, no. 1, pp. 425–443, 2010.

[18] Y. Li and X. Shang, "Multipath ghost target identification for automotive MIMO radar," in *2022 IEEE 96th Vehicular Technology Conference (VTC2022-Fall)*, 2022, pp. 1–5.

[19] L. Zheng, J. Long, M. Lops, F. Liu, X. Hu, and C. Zhao, "Detection of ghost targets for automotive radar in the presence of multipath," *IEEE Transactions on Signal Processing*, vol. 72, pp. 2204–2220, 2024.

[20] R. Takahashi, P. Wang, and K. Suwa, "ESTAR multipath angle estimation for sparse array MIMO radar," in *IEEE International Radar Conference*, 2024.

[21] H. Luo, Z. Zhu, M. Jiang, S. Guo, and G. Cui, "An effective multipath ghost recognition method for sparse MIMO radar," *IEEE Transactions on Geoscience and Remote Sensing*, vol. 61, pp. 1–11, 2023.

[22] R. Takahashi and P. Wang, "GREST: Ghost targets removal algorithm using multipath angle estimation," in *ICASSP 2025 - 2025 IEEE International Conference on Acoustics, Speech and Signal Processing (ICASSP)*, 2025, pp. 1–5.